Feasibility of giant fiber-optic gyroscopes

Stephan Schiller

Institut für Experimentalphysik, Heinrich-Heine-Universitüt Düsseldorf, 40225 Düsseldorf, Germany

(Received 9 May 2012; revised manuscript received 4 January 2013; published 20 March 2013)

The availability of long-distance underground fiber-optic links opens a perspective of implementing interferometric fiber-optic gyroscopes embracing very large areas. We discuss the potential sensitivity, as well as some disturbances and approaches to overcome them.

DOI: 10.1103/PhysRevA.87.033823 PACS number(s): 42.81.Pa, 42.81.Uv

I. INTRODUCTION

Optical gyroscopes are precision instruments widely applied in inertial guidance of airplanes, rockets, and vessels. The scientific applications of gyroscopes include geophysical and general relativity measurements [1–3]. Research-type gyroscopes for the measurement of the fluctuations of the Earth's rotation rate Ω_E have been successfully implemented as active ring laser gyroscopes. In these, counterpropagating laser waves oscillate and generate a beat signal. The ring laser gyroscope at Fundamentalstation Wettzell (Germany) currently exhibits the best long-term stability. It has a ring area $A = 4$ m^2 and reaches approximately 1×10^{-8} relative resolution in Ω_E for integration times of 1–24 h [4,5]. This is made possible by operating the gyroscope in a (passively) very stable laboratory environment and employing active stabilization techniques, which suppress fluctuations of the ring area and of other properties of the gyroscope.

Since the potential sensitivity of gyroscopes scales with the enclosed area, early on large gyroscopes were conceived and implemented, in particular, one reported by Michelson and coworkers in 1925 with enclosed area $A \simeq 0.2$ km^2 and recently a 834-m^2 ring laser gyroscope in New Zealand [6]. In interferometric (passive) fiber-optic gyroscopes [7], a large sensitivity may be achieved in a compact footprint by coiling a fiber with thousands of turns, yielding areas of tens of m^2.

It is of interest to consider alternative approaches to the established ones, for example, in view of increasing the number of operating gyroscopes, and eventually improving the combined signal-to-noise ratio of the measurement of fluctuations of Ω_E. The recent development of long-distance fiber-based optical frequency transfer links [8–10] provides important information for such approaches. These links use commercial or research network underground telecommunication fibers in the 1.5-μm spectral range. In the immediate future, it is intended to use such links to compare atomic clocks located in different laboratories, in order to characterize their performance and to set up a network of clocks implementing a future new definition of the unit of time. It is also foreseen to use comparisons between distant clocks for local measurements of the gravitational potential of the Earth, making use of the general-relativistic effect of time dilation.

In view of these developments, we discuss here whether existing fiber links could enable a complementary application, namely, gyroscopes. That is, we consider applying the concept of the small-scale interferometric fiber gyroscope to an already installed underground fiber network.

II. BASIC CONCEPT

1. Principle

Consider the geometry shown in Fig. 1, which is similar to a usual passive fiber gyroscope. The fiber loop (ring) would in practice be formed by sections of existing underground fiber that are selected to form a closed path, enclosing an area A. From a station, a (frequency-stable) laser wave of angular frequency ω is sent around a fiber loop in the two opposite directions. If the fiber loop is very long, at intervals of approximately 200 km amplifiers are required that coherently amplify the two counterpropagating waves. After their respective round trips, the two waves are brought to interference. The interference signal depends on the Sagnac phase:

$$\Phi_S = 4\,\omega\,\mathbf{A}\cdot\boldsymbol{\Omega}/c^2,$$

which is independent of the index of refraction of the fiber. For example, for a circular loop of circumference $L = 500$ km, assumed for simplicity to be perpendicular to $\boldsymbol{\Omega}$, and for Earth's rotation rate $\Omega = \Omega_E$, the Sagnac phase for a wavelength 1.5 μm is $\Phi_E \simeq 8 \times 10^5$ rad. Usually, the phase itself is not of interest, but its time variations are.

One condition for proper operation of such a large-area fiber interferometer is that the amplifiers introduce only a small nonreciprocal phase shift. This appears to be fulfilled by using the recently demonstrated Brillouin amplifiers [8]. A second condition is that the "fast" fiber length noise—i.e., that due to the spectral components with Fourier frequency larger than $1/T$, where T is the light propagation time around the fiber, which would prevent the two counterpropagating waves from experiencing the same optical path—is sufficiently averaged out. By using a long enough integration time τ, the fiber noise will be common to both light waves. This is discussed in more detail in Sec. III.

2. Signals

Figure 2 shows in more detail the setup considered here. Originating from a common laser source, one wave (a,cw) is injected clockwise into the loop and one wave (b,ccw) is injected counterclockwise. The phases at the ends of their loops are

$$\Phi_{a,\mathrm{cw}} = \tfrac{1}{2}\Phi_S + \Phi(\omega) + \Phi_{K,a,\mathrm{cw}} + \Phi_{T,a,\mathrm{cw}}, \quad (1)$$

$$\Phi_{b,\mathrm{ccw}} = -\tfrac{1}{2}\Phi_S + \Phi(\omega) + \Phi_{K,b,\mathrm{ccw}} + \Phi_{T,b,\mathrm{ccw}}. \quad (2)$$

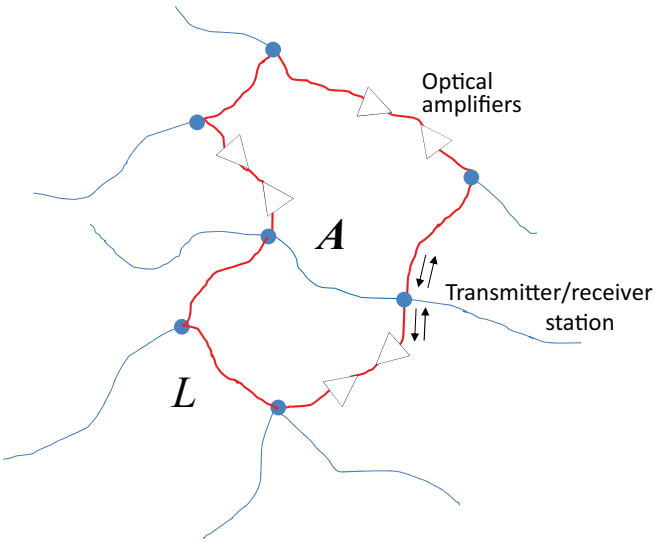

FIG. 1. (Color online) Schematic of a fiber gyroscope using part of an existing fiber network (thick red lines). A wave produced by a laser source in the transmitter node is split and sent around the loop in both directions (black arrows). At the same node the waves are received and interfered with, producing the Sagnac signal. L and A are the loop length and enclosed area, respectively.

Here, Φ_S is the Sagnac phase, $\Phi(\omega) = \int_0^L \beta(\omega) dl$ is the usual propagation phase shift (β is the propagation constant), Φ_K is the Kerr phase shift caused by the presence of the optical

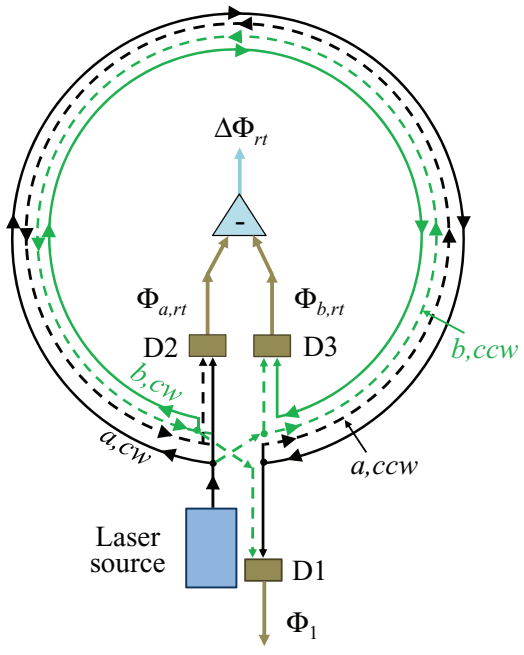

FIG. 2. (Color online) Optical layout of the fiber gyroscope. Four waves of equal frequency are propagating around the loop. Full lines denote clockwise propagating waves, and dashed lines denote counterclockwise propagating ones. D1, D2, and D3 are photodetectors at which interference of two waves occurs. Their signals contain information about relative phases and their time variations. Φ_1 is the phase from which the fluctuations of the Sagnac phase Φ_S is determined.

waves having finite intensity, and Φ_T is a nonreciprocal phase shift of thermal origin (the Shupe effect [11]). At the end of their loop propagations, waves a and b are partially extracted and interfere on a photodetector D1, producing the Sagnac signal. It is given by

$$\begin{aligned}\Phi_1 &= \Phi_{a,\mathrm{cw}} - \Phi_{b,\mathrm{ccw}} \\ &= \Phi_S + (\Phi_{K,a,\mathrm{cw}} - \Phi_{K,b,\mathrm{ccw}}) + (\Phi_{T,a,\mathrm{cw}} - \Phi_{T,b,\mathrm{ccw}}).\end{aligned} \tag{3}$$

Note that it is modified by Kerr and Shupe contributions.

In addition, at the end the loop, each wave is partially reflected (possibly frequency shifted by an acousto-optic modulator) and sent back to the loop beginning. These waves, denoted by a,ccw and b,cw, experience the phase shifts

$$\Phi_{a,\mathrm{ccw}} = -\tfrac{1}{2}\Phi_S + \Phi(\omega) + \Phi_{K,a,\mathrm{ccw}} + \Phi_{T,a,\mathrm{ccw}}, \tag{4}$$

$$\Phi_{b,\mathrm{cw}} = +\tfrac{1}{2}\Phi_S + \Phi(\omega) + \Phi_{K,b,\mathrm{cw}} + \Phi_{T,b,\mathrm{cw}}. \tag{5}$$

From these waves we can form two more signals $\Phi_{a,\mathrm{rt}}$ and $\Phi_{b,\mathrm{rt}}$ at the detectors D2 and D3, respectively, which carry information about the round-trip phases:

$$\begin{aligned}\Phi_{a,\mathrm{rt}} &= \Phi_{a,\mathrm{cw}} + \Phi_{a,\mathrm{ccw}} \\ &= 2\Phi(\omega) + \Phi_{K,a,\mathrm{cw}} + \Phi_{K,a,\mathrm{ccw}} + \Phi_{T,a,\mathrm{cw}} + \Phi_{T,a,\mathrm{ccw}},\end{aligned} \tag{6}$$

$$\begin{aligned}\Phi_{b,rt} &= \Phi_{b,\mathrm{cw}} + \Phi_{b,\mathrm{ccw}} \\ &= 2\Phi(\omega) + \Phi_{K,b,\mathrm{cw}} + \Phi_{K,b,\mathrm{ccw}} + \Phi_{T,b,\mathrm{cw}} + \Phi_{T,b,\mathrm{ccw}}.\end{aligned} \tag{7}$$

A stabilized fiber is one in which one of these two, say, $\Phi_{a,\mathrm{rt}}$, is measured and kept constant in time by active feedback.

Finally we can form (electronically) the difference round-trip phase:

$$\begin{aligned}\Delta\Phi_{\mathrm{rt}} &= \Phi_{a,\mathrm{rt}} - \Phi_{b,\mathrm{rt}} \\ &= (\Phi_{T,a,\mathrm{cw}} + \Phi_{T,a,\mathrm{ccw}}) - (\Phi_{T,b,\mathrm{ccw}} + \Phi_{T,b,\mathrm{cw}}) \\ &\quad + (\Phi_{K,a,\mathrm{cw}} + \Phi_{K,a,\mathrm{ccw}}) - (\Phi_{K,b,\mathrm{cw}} + \Phi_{K,b,\mathrm{ccw}}).\end{aligned} \tag{8}$$

This signal carries information only about disturbances.

III. SENSITIVITY

Consider the state-of-the-art long-buried-fiber link ($L =$ 480 km) of Terra *et al.* [8], at the wavelength 1.5 μm. In effect, they have implemented a device that can measure the Sagnac phase, although their loop had essentially zero enclosed area. It is not a conventional Sagnac interferometer with counterpropagating waves for which the propagation phases cancel, but a single-wave geometry in which the round-trip propagation phase $\Phi_{a,\mathrm{rt}}$ is kept constant by fiber stabilization. The crucial measurement performed by them in this context is the phase noise present on the wave traversing the stabilized link once (i.e., half a round trip), i.e., on the signal $\Phi_{a,\mathrm{cw}}$. This is equivalent, in the absence of the Shupe and Kerr effect contributions, to one half the phase noise of the Sagnac signal Φ_S. Terra *et al.* measured a spectral noise density $S_D(f) \simeq 2 \times 10^{-2}\,\mathrm{rad}^2/\mathrm{Hz}$ for $0.1 < f < 1$ Hz. It may be assumed that this value holds also for lower frequencies f,

since the fiber is stabilized. Thus, the phase error incurred over an integration time τ is $\sigma_\Phi(\tau) \simeq 0.14\,\mathrm{rad}/(\tau/1\,\mathrm{s})^{1/2}$. The corresponding relative sensitivity of the Earth's rotation rate measurement is $\sigma_\Phi(\tau)/\Phi_E \simeq 1.8 \times 10^{-7}/(\tau/1\,\mathrm{s})^{1/2}$. If this noise would average down ideally, for a one-day-long integration ($\tau = 24$ h) the extrapolated relative resolution of the Earth's rotation rate would be 6×10^{-10}. The nonorthogonality of the loop and Earth's rotation axes and the above factor one half will moderately increase this number.

It has been predicted [12] and confirmed for $L < 500$ km [8] that S_D and therefore σ_Φ scale as $L^{3/2}$. The Sagnac phase, however, scales as L^2 for a circular loop. Thus, the relative resolution could improve for longer fiber links as $L^{-1/2}$, if no other unexpected effects show up.

IV. DISTURBANCES

A. Stability of the loop area

The expression for the Sagnac phase shows that reaching a desired sensitivity for determining changes in Ω requires the instability of the frequency ω and of the enclosed area A to be correspondingly small over the desired integration time. The frequency ω can be kept constant to the 10^{-15} relative level or better by stabilizing the laser frequency to an atomic clock reference, so this influence is negligible. However, an active stabilization of the area A does not seem possible, due to lack of a way of directly determining the area (independently from measuring the Sagnac effect). The following considerations indicate the relevance of variations of A and approaches which may be useful in reducing them.

The first approach relies on the passive stability of the fiber. Consider the fiber length L (ring perimeter) stability as an indicator of enclosed area stability. Fibers that are installed underground are "quiet" with respect to their optical length noise. Several groups have characterized the level of frequency instability achievable in optical carrier wave transmission along long, unstabilized fiber links. Terra *et al.* [8] measured the relative frequency instability $\sigma_y(\tau)$ imposed on an optical wave after passage through a 480-km unstabilized, dark fiber link to be 6×10^{-15} or less for integration times τ between 10 and 500 s, the longest integration time reported in their study. Kéfélian *et al.* [9] observed a roughly constant level below 1×10^{-14} for τ up to 100 000 s in a 108-km-long fiber link. Lopez *et al.* [10] measured a similar level for 150 km of telecommunication fiber carrying internet data. The corresponding optical phase instability is approximately $\delta\Phi \simeq \omega\tau\,\sigma(\tau)$. For the first example, $\delta\Phi \simeq 4 \times 10^3$ rad at $\tau =$ 500 s and is correspondingly higher at longer integration times. Referred to a $L = 500$-km length, this implies a relative instability of the optical path length of $\delta(nL)/nL \simeq \delta\Phi/\Phi \simeq 4 \times 10^3/[2\pi \times 1.45 \times 5 \times 10^5\,\mathrm{m}/(1.5\,\mu\mathrm{m})] \simeq 1 \times 10^{-9}$ at $\tau =$ 500 s (n is the refractive index of the fiber). It is dominated by fluctuations of the index of refraction of the fiber, whose temperature sensitivity is significantly larger than that of the length. At first sight, the above value would indicate a relative area instability of less than 1×10^{-9} for integration times up to 500 s. However, there may be area variations not related to perimeter length variations, e.g., caused by ground movement. Assume for simplicity a circular ring. Requiring an area instability $\delta A/A < 1 \times 10^{-9}$ (a necessary condition if an Earth's rotation rate sensitivity better than the best gyroscopes is aimed for) for a ring of $R = 100$ km leads to the requirement $\delta R < 50\ \mu$m for the (ring-averaged) radius change. Such a level appears realistic over sufficiently short time intervals (several minutes). The level of instability of the area over medium and long averaging times is of fundamental importance and should be determined experimentally.

The second approach is an active one. The optical phase accumulated over the loop (ignoring the Sagnac phase) may be written as

$$\Phi(\omega) = c^{-1}\omega \int_0^L n(\omega, s(l), T(l))\, dl,$$

where the dependence of the fiber index on the strain s and on the temperature T along the fiber has been introduced. A Taylor expansion of the integral for small but position-dependent variations in the fiber length, the strain, and the temperature around their respective mean values L_0, s_0, and T_0 yields the phase deviation as

$$\delta\Phi(\omega) \simeq c^{-1}\omega\Big(n(\omega,s_0,T_0)\delta L + n_s(\omega,s_0,T_0)\int_0^L \delta s(l)dl + n_T(\omega,s_0,T_0)\int_0^L \delta T(l)dl\Big). \quad (9)$$

δL denotes the overall length variation. The subscripts s and T indicate partial derivatives of the refractive index with respect to strain and temperature, respectively. Note that the refractive index depends on the optical frequency ω, but its derivatives do as well. Consider sending three sufficiently spaced frequencies ω_1, ω_2, and ω_3 (which should lie in the spectral region in which the fiber has low propagation loss and for which optical amplifiers are available) around the ring and measuring the three corresponding phase deviations $\delta\Phi(\omega_1)$, $\delta\Phi(\omega_2)$, and $\delta\Phi(\omega_3)$ as a function of time. In order not to accumulate Sagnac phases, the measurement is done by sending the waves around the ring and back the same way (as in fiber link stabilization procedures), whereby each total phase is twice the single-turn phase (after fast fluctuations are averaged out). The corresponding signal is given in Eqs. (6) and (7). By linear combination of the three phase deviations $\delta\Phi(\omega_i)$ with weights determined by the refractive index partial derivatives, we may extract information about the loop length variation δL. This variation may be actively compensated using, e.g., a special piece of fiber being part of the ring, whose temperature or strain can be actively modified. Based on the achievements in long-distance fiber links it is expected that the fiber geometrical length L can be stabilized to a relative level far below 1×10^{-12} for all relevant integration times. This stabilization could be helpful in reducing also the area fluctuations, and this hypothesis should be tested experimentally. However, the link stabilization cannot compensate variations of the encompassed area A that are not due to variations of the link length L. It should be noted that this approach is conceptually related to the active perimeter stabilization implemented in the large ring laser gyroscope [4].

We suggest as a third approach a more complicated link network to reject area variations, shown in Fig. 3 (left). In it, one link is added which splits the original area A in two

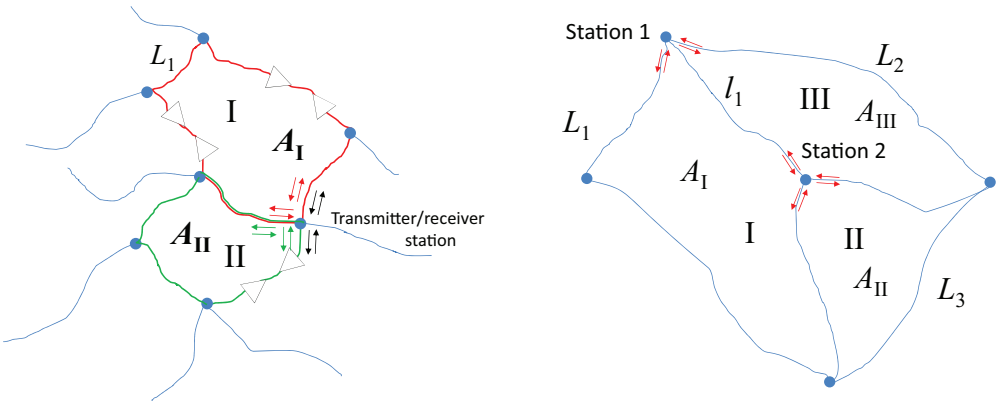

FIG. 3. (Color online) Proposed fiber network geometries for the discrimination of area changes. Left: simplest geometry with three gyroscopes I, II, and I-II. The laser waves traveling in these three gyroscopes from the single station are indicated by the red, green, and black arrows, respectively. Right: more complex geometry. Station 1 operates the outer fiber loop enclosing areas A_{I}, A_{II}, and A_{III}. Station 2 operates (possibly alternating) the three smaller individual loops I, II, and III. Laser waves are indicated by arrows, but are not color coded. For example, a change in the outer loop area by deformation of the outer loop link subsection L_1 can be detected and rejected by correlation with the Sagnac signal from gyroscope I and noncorrelation with signals from gyroscopes II and III. If instead a deformation of the link subsection l_1 occurs, this would not appear in the outer gyroscope signal but could nevertheless be detected by anticorrelation between the signals from gyroscopes I and III and noncorrelation between the signals from gyroscope I and gyroscope II.

approximately equal parts A_{I} and A_{II}. This results in three gyroscopes I, II, and the combined loop I-II, which can be operated independently, either simultaneously or alternating. Consider now a change in area of the combined gyroscope I-II due to a spatial displacement of link section L_1. This will result in a signal in the I-II gyroscope but also in the smaller gyroscope I, while not in the gyroscope II. By detecting such a signature, the signal on the I-II gyroscope would be identified as a disturbance. A similar reasoning applies if the I-II gyroscope area changes due displacement of other sections. In contrast, a change in rotation rate Ω yields a common (but unequal) signal on all three gyroscopes. The sensitivities of the three gyroscopes to rotation differ because of the different areas, but these areas can be computed from a measurement of the geometry (e.g., using GPS) and taken into account in the disturbance rejection analysis.

More complicated geometries can be considered, e.g., the one shown in Fig. 3 (right), containing two stations and four gyroscopes. With such geometries, the rejection of disturbances might be even more effective.

In addition to the instability of the enclosed area we point out that the Sagnac phase contains the scalar product $\mathbf{A}\cdot\mathbf{\Omega}$. Variations in the orientation of the fiber loop with respect to the Earth's axis will thus also produce signals. These signals may be undesired for some applications but possibly useful for others.

B. Nonreciprocal errors

1. *Shupe effect*

The Shupe effect [11] is caused by the presence of a time-dependent inhomogeneous temperature distribution in the fiber. In a conventional fiber-optic gyroscope, there are two counterpropagating waves. The wave trains reaching the detector at the same time have crossed every section of the fiber loop, except the one at the mid-point, at a different time. At the two times of passage the respective values of the temperature will differ (due to temperature drift), causing a different phase shift for the two waves due to the finite thermo-optic coefficient dn/dT and the fiber thermal expansion coefficient α. The differential phase accumulates over the length of the fiber, giving rise to a nonreciprocal phase shift Φ_T which adds to the Sagnac phase. As the temperature drift dT/dt is not constant in time, Φ_T and therefore the total phase change with time. According to the model given by Shupe, the time interval $\tau_{\text{cc-ccw}}$ between the passages of the clockwise and counterclockwise wave through a fiber section located at a distance l from one end is given by $\tau_{\text{cc-ccw}} = \beta(2\,l - L)/\omega$, where β is the propagation constant. Then, the total nonreciprocal phase is

$$\begin{aligned}\Phi_{1,T} &= \Phi_{T,a,\text{cw}} - \Phi_{T,b,\text{ccw}} \\ &\simeq k(dn/dT + n\alpha)\int_0^L \tau_{\text{cc-ccw}}[dT(l)/dt]dl \\ &\simeq (n\omega/c^2)(dn/dT + n\alpha)\int_0^L (2l - L)[dT(l)/dt]dl.\end{aligned} \tag{10}$$

Here, $\beta \simeq k\,n = n\,\omega/c$ has been used. Note that $\Phi_{1,T}$ vanishes if the temperature change rate is constant over the fiber length. A model assumption for the inhomogeneous temperature change in the fiber discussed by Shupe is $dT(l)/dt = (\Delta T/\Delta t)(l/L)$. Shupe proposed and studies have been performed on particular winding (coiling) geometries in order to reduce the effect. These special geometries are obviously not applicable here.

In order to model the Shupe effect for a long buried fiber, we divide the length L into N intervals, each of which has a particular temperature drift rate uncorrelated with that of the other intervals. The temperature drift rates are assumed to have a Gaussian random distribution with zero mean and standard deviation $\sigma_{dT/dt} = 0.1$ K/h, a typical value for buried fibers [8]. A numerical modeling shows

that the total phase also has a Gaussian distribution with zero mean and a standard deviation approximately given by $\sigma_T \simeq \sigma_{dT/dt}\sqrt{N}L^2k\,(dn/dT + n\alpha)/c$. For a loop length $L = 500\,\mathrm{km}$ and $N = 500$ intervals, $\sigma_T \simeq 22$ rad. This is a large value, and time-varying temperature drift rates will overwhelm any Earth's rotation rate fluctuation signal.

Consider now the configuration used in fiber noise cancellation (Fig. 2): a wave running in one direction around the loop, reflected back at the end and returning to the emitter. Now, the sum of time delays for reaching the same fiber section l on the forward and backward trips is always $\beta(2L)/\omega$. Therefore $\Phi_{T,a,\mathrm{cw}} + \Phi_{T,a,\mathrm{ccw}} = \Phi_{T,b,\mathrm{cw}} + \Phi_{T,b,\mathrm{ccw}} \propto (\beta(2L)/\omega)\int_0^L (dT(l)/dt)dl$. The difference $\Delta\Phi_{\mathrm{rt}}$ between the two round-trip phases, introduced above in Eq. (8), is therefore independent of the Shupe effect and only contains information about the Kerr effect.

For concreteness, we explicitly state the Shupe effect contributions for the four one-way propagation phases introduced in Eqs. (1), (2), (4), and (5):

$$\begin{aligned}
\Phi_{a,\mathrm{cw}}(\omega) &= \frac{1}{2}\Phi_S + \Phi(\omega) + \xi\int_0^L l\,T_t\,dl + \Phi_{K,a,\mathrm{cw}},\\
\Phi_{b,\mathrm{ccw}}(\omega) &= -\frac{1}{2}\Phi_S + \Phi(\omega) + \xi\int_0^L (L-l)T_t\,dl + \Phi_{K,b,\mathrm{ccw}},\\
\Phi_{a,\mathrm{ccw}}(\omega) &= -\frac{1}{2}\Phi_S + \Phi(\omega) + \xi\int_0^L (2L-l)T_t\,dl + \Phi_{K,a,\mathrm{ccw}},\\
\Phi_{b,\mathrm{cw}}(\omega) &= +\frac{1}{2}\Phi_S + \Phi(\omega) + \xi\int_0^L (L+l)T_t\,dl + \Phi_{K,b,\mathrm{cw}}.
\end{aligned} \tag{11}$$

Here we have introduced the parameter $\xi(\omega) = (n(\omega)\omega/c^2)[dn(\omega)/dT + n(\omega)\alpha]$ and the short-hand notation $T_t = dT(l)/dt$. Φ_K are Kerr phases discussed further below. We see that $\Phi_S/2$ always occurs in combination with $\xi\int lT_t dl$. This part of the Shupe contribution is therefore always measured together with the Sagnac phase. It is not possible to determine Φ_S alone from any linear combination of the above four phases.

Returning to the Sagnac signal, Eq. (3), we ignore the Kerr effect for the time being and have

$$\begin{aligned}
\Phi_1(\omega) &= \Phi_{a,\mathrm{cw}}(\omega) - \Phi_{b,\mathrm{ccw}}(\omega)\\
&= \Phi_S + \xi(\omega)\int_0^L (2l-L)T_t dl.
\end{aligned} \tag{12}$$

Although both Φ_S and $\xi(\omega)$ are proportional to ω, the latter coefficient has an additional (weak) dependence on ω through the factor $n(\omega)[dn(\omega)/dT + n(\omega)\alpha]$. Therefore, we can again consider the possibility of using waves of different frequencies ω. With two frequencies, we may produce the signals $\Phi_1(\omega_1)$ and $\Phi_1(\omega_2)$. They are not linearly dependent, and we may produce an appropriate linear combination and extract the Sagnac phase $\Phi_S(\omega)$ and the Shupe contribution $\int_0^L (2l-L)T_t\,dl$ independently.

Thus, it is in principle possible to measure the Shupe effect of the standard Sagnac configuration by measuring at different optical frequencies, at least if we neglect the influence of the Kerr effect. It therefore should be possible to correct for the Shupe effect, although to what level is a question that experiments have to answer. This correction is compatible with active stabilization of one of the two round-trip phases.

2. *Optical Kerr effect*

The intensity of any wave propagating inside a fiber changes the refractive index via the optical Kerr effect. In the standard Sagnac geometry with two counterpropagating waves of powers P_{cw} and P_{ccw}, there arises a nonzero differential phase shift $\Phi_{K,\mathrm{cw}} - \Phi_{K,\mathrm{ccw}}$ if the average powers of the two waves are not equal, since for each fiber length interval dl there arises both a self-Kerr phase shift and a cross-Kerr phase shift (which has an additional factor of 2), given by $d\Phi_{K,\mathrm{cw}} = \kappa(P_{\mathrm{cw}} + 2\,P_{\mathrm{ccw}})dl$ and $d\Phi_{K,\mathrm{ccw}} = \kappa(P_{\mathrm{ccw}} + 2\,P_{\mathrm{cw}})dl$, where κ is the Kerr coefficient [3]. Obviously, the solution to this problem consists in equalizing the two powers P_{cw} and P_{ccw} by appropriate means, and this has been implemented experimentally by several groups [3]. Another approach, recently demonstrated [13], is the use of a photonic crystal fiber instead of a standard fiber, but this solution is not compatible with already installed fibers and also exhibits much higher fiber loss. For a long-distance fiber link, where optical amplifiers are present, the situation becomes more complex. For example, in the approach of using Brillouin amplification [8], the power $P^{(p)}$ of the pump waves injected into the fiber (of the order of tens of mW) also induces a change of the index of refraction. However, the effect on the phases of the two counterpropagating waves is equal because it is a cross-Kerr effect, $\Phi^{(p)}_{K,\mathrm{cw}} = \Phi^{(p)}_{K,\mathrm{ccw}} = \Phi^{(p)}_K = \kappa\int_0^L 2P^{(p)}(l)dl$, and this particular Kerr contribution cancels in the standard Sagnac geometry.

We now extend the discussion to the configuration of Fig. 2. We take into account that in each fiber section there are five waves present: the pump wave (p) (there is no need to differentiate the contributions in the clockwise and counterclockwise directions; only the total power is considered) and the four "signal" waves a,cw, a,ccw, b,cw, and b,ccw , each with arbitrary position-dependent powers. Therefore,

$$\begin{aligned}
\Phi_{K,a,\mathrm{cw}} = \kappa\int_0^L (&P_{a,\mathrm{cw}} + 2P_{a,\mathrm{ccw}} + 2P_{b,\mathrm{cw}} + 2P_{b,\mathrm{ccw}}\\
&+ 2P^{(p)})dl,
\end{aligned}$$

and the same applies analogously for the other three signal waves. The Kerr contributions to the Sagnac signals are therefore

$$\Phi_{1,K} = \Phi_{K,a,\mathrm{cw}} - \Phi_{K,b,\mathrm{ccw}} = \kappa\int_0^L (-P_{a,\mathrm{cw}} + P_{b,\mathrm{ccw}})dl, \tag{13}$$

$$\Phi_{2,K} = \Phi_{K,b,\mathrm{cw}} - \Phi_{K,a,\mathrm{ccw}} = \kappa\int_0^L (-P_{b,\mathrm{cw}} + P_{a,\mathrm{ccw}})dl. \tag{14}$$

For the round-trip phase difference introduced in Eq. (8), we have

$$\begin{aligned}
\Delta\Phi_{\mathrm{rt}} &= (\Phi_{K,a,\mathrm{cw}} + \Phi_{K,a,\mathrm{ccw}}) - (\Phi_{K,b,\mathrm{cw}} + \Phi_{K,b,\mathrm{ccw}})\\
&= \kappa\int_0^L (-P_{a,\mathrm{cw}} - P_{a,\mathrm{ccw}} + P_{b,\mathrm{cw}} + P_{b,\mathrm{ccw}})dl.
\end{aligned} \tag{15}$$

This signal is certainly useful for monitoring how large the fluctuations of the average powers are.

How do we perform active stabilization of one of the Kerr contributions, say, $\Phi_{1,K}$? Ideally, we would measure and control both length-averaged powers $\int_0^L P_{a,\mathrm{cw}} dl$ and $\int_0^L P_{b,\mathrm{ccw}} dl$. But these average values appear not to be easily measurable. For example, if we turn off alternating either wave a,cw or b,ccw in order to determine its effect in the Sagnac signal Φ_1 or on $\Delta\Phi_{\mathrm{rt}}$, we also lose these signals. We may instead reduce the input power of the a,cw and of the b,ccw waves by a fixed fraction (as set by an accurate power measurement). This will not necessarily reduce the average power by the same fraction, since inside the fiber, the powers in various sections will not be strictly linearly dependent on the input power, due to saturation effects in the amplification stages. Nevertheless, the difference in the signal with full and reduced power might be used as the quantity that is kept constant by acting back on the input power.

Another option is to stabilize the a,cw and b,ccw powers exiting the fibers and reaching the detectors. A test of the suitability of this approach could be performed by implementing this stabilization for the four waves appearing in Eq. (15) and characterizing the resulting stability of $\Delta\Phi_{\mathrm{rt}}$.

It seems possible to extend these procedures to the case of the use of multiple frequencies considered in Sec. IV B1.

In another potential solution, one is led to measure the powers at several locations along the loop and stabilize their values actively, e.g., by using a feedback servo on the amplifier pump source closest to the measurement point (note that Brillouin amplification is unidirectional) or to the laser source. While it is possible to distinguish between the clockwise and counterclockwise waves using directional couplers, it is less straightforward to distinguish between the waves a and b running in the same direction, as they have nearly the same frequency. One possibility consists in amplitude modulating with different frequencies the two waves a,cw and b,ccw before entering the fiber and detecting the corresponding power modulation signals.

3. Other effects

Other noise sources exist in fiber gyroscopes, such as Rayleigh backscattering. The scaling derived for the usual fiber gyroscopes [3] indicates that the effect is strongly reduced for large rings. The link stabilization technique will compensate for changes in the effect arising from the round-trip wave propagation, but the rotation signal will have a contribution that depends only on the counterclockwise wave propagation. Thus the stabilization technique does not appear to provide a means to compensate for the effect. However, modulation techniques that have been suggested for fiber gyroscopes should also be applicable to giant rings.

V. CONCLUSION

In this paper, we proposed the use of optical fibers belonging to installed underground fiber networks for an implementation of gyroscopes with potentially high sensitivity, thanks to the giant encompassed area, on the order of 10^{10} m^2. The stability of the gyroscope is of crucial importance if a high sensitivity is to be attained. While a study of the perturbations affecting large ring laser structures has uncovered difficulties [6], it is here suggested that in a stabilized buried fiber-based gyroscope the perturbations may be of a different type. The most basic requirements for the implementation were discussed.

The need for optical amplifiers that do not produce significant nonreciprocal time-varying phases was pointed out and seems feasible.

It was furthermore pointed out that the Shupe effect may be measured using a multifrequency approach, allowing us to correct the Sagnac signal which is affected by it. No elegant measurement concept for determining the Kerr effect was found, so that an indirect technique is required instead. Approaches considered for achieving an approximate stabilization of the relevant loop-averaged powers are a pointwise stabilization of each wave's power, an output power stabilization, and a stabilization of the round-trip phase difference.

A further crucial requirement is a time-stable enclosed area A. The level of instability of large fiber loop areas has not been measured so far, to the author's knowledge, and and should be determined experimentally. A gyroscope that aims at being a competitive instrument for Earth's rotation rate studies requires a relative area instability of 1×10^{-9} or less (i.e., an area variation not larger than on the order of 10 m^2 for a giant fiber loop). It is an open issue whether this is achievable, but even a much higher instability could lead to useful applications, since a giant fiber gyroscope implements an averaging over a larger area and thus a different kind of measurement as compared to conventional instruments. In the best case, the passive stability of buried fibers will provide sufficient area stability due to averaging of disturbances over a large spatial scale, in particular, if the measurement can be performed within a sufficiently short time. This would come at the expense of sensitivity, however, since a short averaging time does not allow us to average down the noise significantly.

In another, still favorable case, there might be a partial correlation between area change and geometric path length change, in which case a measurement of length fluctuations and their active compensation or correction could represent a partial solution. Extensions of long-distance fiber link stabilization techniques, aiming to stabilize the geometric path length L instead of the optical path length $n\,L$, are suggested for this purpose.

As a third option, more complex fiber network gyroscope geometries might be helpful for spurious signal rejection due to area changes. They require more but not fundamentally different infrastructure as compared to the simplest ring geometry. The latter two approaches may be helpful in achieving low gyroscope instability also on long time scales.

Finally, it is suggested that experimental studies are undertaken to verify the concepts proposed here. To be specific, it is desirable to extend the noise measurements performed by Terra *et al.* [8] to lower frequencies, to verify the suggestion of dual frequency use for extraction of the Shupe effect and the use of three frequencies for length stabilization, to measure the Kerr-effect-induced phase fluctuations, and to verify the feasibility of the power stabilization procedures sketched here.

Note added in proof. Recently, the first experimental realization of a large-area fiber Sagnac interferometer using

existing telecom fiber links has been reported by Clivati *et al.* [14]. The 20-km^2-area gyroscope exhibits a noise floor of $\sigma_{\Phi_S}(\tau > 20\,\mathrm{s})/\Phi_E \simeq 4 \times 10^{-5}$ relative to the Earth's rotation rate.

ACKNOWLEDGMENTS

I thank A.Yu. Nevsky and I. Ernsting for comments on the manuscript.

[1] G. E. Stedman, Rep. Prog. Phys. **60**, 615 (1997).
[2] F. Bosi *et al.*, Phys. Rev. D **84**, 122002 (2011).
[3] W. W. Chow, J. Gea-Banacloche, L. M. Pedrotti, V. E. Sanders, W. Schleich, and M. O. Scully, Rev. Mod. Phys. **57**, 61 (1985).
[4] K. U. Schreiber, T. Klügel, J. P. R. Wells, R. B. Hurst, and A. Gebauer, Phys. Rev. Lett. **107**, 173904 (2011).
[5] http://www.wettzell.ifag.de/LKREISEL/G/LaserGyros.html
[6] R. B. Hurst, G. E. Stedman, K. U. Schreiber, R. J. Thirkettle, R. D. Graham, N. Rabeendran, and J.-P. R. Wells, J. Appl. Phys. **105**, 113115 (2009).
[7] H. C. Lefèvre, Opt. Rev. **4**, A20 (1997).
[8] O. Terra, G. Grosche, and H. Schnatz, Opt. Express **18**, 16102 (2010).
[9] F. Kéfélian, O. Lopez, H. Jiang, C. Chardonnet, A. Amy-Klein, and G. Santarelli, Opt. Lett. **34**, 1573 (2009).
[10] O. Lopez, A. Haboucha, F. Kéfélian, H. Jiang, B. Chanteau, V. Roncin, C. Chardonnet, A. Amy-Klein, and G. Santarelli, Opt. Express **18**, 16849 (2010).
[11] D. M. Shupe, Appl. Opt. **19**, 654 (1980).
[12] W. Williams, W. C. Swann, and N. R. Newbury, J. Opt. Soc. Am. B **25**, 1284 (2008).
[13] V. Dangui, M. J. F. Digonnet, and G. S. Kino, Opt. Lett. **34**, 875 (2009).
[14] C. Clivati, D. Calonico, G. A. Costanzo, A. Mura, M. Pizzocaro, and F. Levi, arXiv:1212.5717.